



1 **Biomass Burning Aerosol as a Modulator of Droplet Number in the Southeast**  
2 **Atlantic Region**

3

4 Mary Kacarab<sup>1</sup>, K. Lee Thornhill<sup>2</sup>, Amie Dobracki<sup>3</sup>, Steven G. Howell<sup>3</sup>, Joseph R.  
5 O'Brien<sup>4</sup>, Steffen Freitag<sup>3</sup>, Michael R. Poellot<sup>4</sup>, Robert Wood<sup>5</sup>, Paquita Zuidema<sup>6</sup>, Jens  
6 Redemann<sup>7</sup>, and Athanasios Nenes<sup>1,8,9</sup>

7

8 <sup>1</sup>School of Earth & Atmospheric Sciences, Georgia Institute of Technology, Atlanta, GA,  
9 30332, USA

10 <sup>2</sup>NASA Langley Research Center, Hampton, VA, 23666, USA

11 <sup>3</sup>Department of Oceanography, University of Hawaii, Honolulu, HI, 96822, USA

12 <sup>4</sup>Atmospheric Sciences Department, University of North Dakota, Grand Forks, ND, 58202,  
13 USA

14 <sup>5</sup>Atmospheric Sciences, University of Washington, Seattle, WA, 98195, USA

15 <sup>6</sup>Department of Atmospheric Sciences, Rosenstiel School of Marine and Atmospheric  
16 Science, University of Miami, Miami, FL, 33149, USA

17 <sup>7</sup>School of Meteorology, University of Oklahoma, Norman, OK, 73072, USA

18 <sup>8</sup>Institute for Chemical Engineering Sciences, Foundation for Research and Technology  
19 Hellas, Patras, GR-26504, Greece

20 <sup>9</sup>Laboratory of Atmospheric Processes and their Impacts, School of Architecture, Civil and  
21 Environmental Engineering, Ecole Polytechnique Federale de Lausanne, Lausanne, CH-  
22 1015, Switzerland

23

24 Corresponding Author: Athanasios Nenes (athanasios.nenes@epfl.ch)

25

26



27 **Abstract**

28 The southeastern Atlantic (SEA) and its associated cloud deck, off the west coast of central  
29 Africa, is an area where aerosol-cloud interactions can have a strong radiative impact.  
30 Seasonally, extensive biomass burning (BB) aerosol plumes from southern Africa reach  
31 this area. The NASA ObseRvations of Aerosols above Clouds and their intEractionS  
32 (ORACLES) study focused on quantitatively understanding these interactions and their  
33 importance. Here we present measurements of cloud condensation nuclei (CCN)  
34 concentration, aerosol size distribution, and vertical updraft velocity in and around the  
35 marine boundary layer (MBL) collected by the NASA P-3B aircraft during the August  
36 2017 ORACLES deployment. BB aerosol levels vary considerably but systematically with  
37 time; high aerosol concentrations were observed in the MBL ( $800\text{-}1000\text{ cm}^{-3}$ ) early on,  
38 decreasing mid-campaign to concentrations between  $500\text{-}800\text{ cm}^{-3}$ . By late August and  
39 early September, relatively clean MBL conditions were sampled ( $<500\text{ cm}^{-3}$ ). These data  
40 then drive a state-of-the-art droplet formation parameterization, from which the predicted  
41 cloud droplet number and its sensitivity to aerosol and dynamical parameters are derived.  
42 Droplet closure was achieved to within 20%. Droplet formation sensitivity to aerosol  
43 concentration, vertical updraft velocity, and the hygroscopicity parameter,  $\kappa$ , vary and  
44 contribute to the total droplet response in the MBL clouds. When aerosol concentrations  
45 exceed  $\sim 900\text{ cm}^{-3}$  and maximum supersaturation approaches 0.1%, droplet formation in  
46 the MBL enters a “velocity-limited” droplet activation regime, where cloud droplet number  
47 responds weakly to CCN concentration increases. Below  $\sim 500\text{ cm}^{-3}$ , in a “clean” MBL,  
48 droplet formation is much more sensitive to changes in aerosol concentration than to  
49 changes in vertical updraft. In the “competitive” regime, where the MBL has



50 “intermediate” pollution ( $500\text{-}800\text{ cm}^{-3}$ ), droplet formation becomes much more sensitive  
51 to hygroscopicity ( $\kappa$ ) variations than for clean and polluted conditions. Higher  
52 concentrations increase the sensitivity to vertical velocity by more than ten-fold. We also  
53 find that characteristic vertical velocity plays a very important role in driving droplet  
54 formation in a more polluted MBL regime, in which even a small shift in  $w^*$  may make a  
55 significant difference in droplet concentrations. Identifying regimes where droplet number  
56 variability is primarily driven by updraft velocity and not aerosol concentration is key for  
57 interpreting aerosol indirect effects, especially with remote sensing. Droplet number  
58 responds proportionally to changes in characteristic velocity, offering the possibility of  
59 remote sensing of  $w^*$  under velocity-limited conditions.  
60



61 **1. Introduction**

62 Aerosol particles affect the planetary radiative balance by directly absorbing and  
63 scattering radiation. They also provide the nuclei upon which cloud droplets and ice  
64 crystals form; variations thereof can profoundly impact cloud formation, precipitation, and  
65 the hydrological cycle (Boucher et al., 2013; Myhre et al., 2013). These aerosol impacts  
66 are thought to be important but uncertain modulators of regional and global scale climate.  
67 The interactions of aerosols with clouds are especially uncertain, and affect estimates of  
68 equilibrium climate sensitivity and transient climate response to greenhouse gas  
69 concentrations (Seinfeld et al., 2016, IPCC 2013).

70 Only a fraction of aerosol can affect clouds; those aerosols that can activate to form  
71 cloud droplets (termed cloud condensation nuclei, CCN) must satisfy a certain range of  
72 physical size and chemical composition for the levels of water vapor supersaturation that  
73 develop in cloud-forming air parcels (Köhler, 1936; Seinfeld and Pandis, 2006). The  
74 properties and dynamical development of warm and mixed-phase clouds are sensitive to  
75 the number of cloud droplets formed. It is now established that anthropogenic emissions  
76 have strongly modulated global CCN and droplet number since the industrial revolution  
77 (e.g., Boucher et al., 2013; Raatikainen et al., 2013). Much work remains, however, to  
78 reduce the uncertainty associated with this forcing on climate (e.g., Seinfeld et al., 2016).

79 Appropriately capturing the variability in droplet number, and its sensitivity to  
80 aerosol (which is at the heart of aerosol-cloud interactions) requires a good description of  
81 aerosol size distribution and hygroscopicity (e.g., Fanourgakis et al., 2019), especially in  
82 boundary-layer clouds where liquid clouds and their radiative cooling dominates. Key  
83 towards achieving this goal is to capture the source characteristics of major aerosol types,



84 and their chemical/microphysical evolution throughout their atmospheric residence.  
85 Biomass burning (BB) aerosol has emerged as a major source of regional and global  
86 aerosol, contributing up to 64% of global surface CCN concentrations (Spracklen et al.,  
87 2011). The influence of BB is expected to increase in importance as the combustion of  
88 biomass (natural and anthropogenic) is expected to accelerate in the future, especially in  
89 Africa, while anthropogenic emissions decrease (Bond, et al. 2013, Andela et al., 2017).

90       Almost one third of annual global biomass burning emissions originate from  
91 regional fires across the savannah and woodlands of sub-Saharan Africa, and one fourth  
92 originate from southern Africa (van der Werf et al., 2010). From approximately June until  
93 October, these intense BB emissions are subsequently transported over the southeast  
94 Atlantic (SEA) region (Adebiyi and Zuidema, 2016; Garstang et al., 1996), greatly  
95 elevating CCN levels above background concentrations (Ross, et al., 2003) and interacting  
96 with low-level marine boundary layer clouds that are abundant in the SEA (e.g., Seager et  
97 al., 2003; Grosvenor et al., 2018; Zuidema et al., 2018). The SEA experiences a structure  
98 transition from marine stratocumulus to trade wind cumulus clouds, so the coincidence of  
99 large BB aerosol plumes implies a potentially large role for aerosol-cloud interactions to  
100 affect cloud radiative properties over a globally-relevant system, potentially modulating  
101 the extent of each regime and the transition itself (Yamaguchi et al., 2015; Zhou et al.,  
102 2017). The microphysical influence of BB aerosol on clouds, however, is non-linear, as  
103 increasing aerosol levels enhance the competition of CCN for water vapor, to the point  
104 where droplet formation may be insensitive to CCN concentration level (e.g., Rissman et  
105 al., 2004; Ruetter et al., 2009; Bougiatioti, et al., 2016). Dynamical adjustments (primarily  
106 vertical velocity) may also respond to CCN and cloud droplet number changes - therefore



107 it is important to quantify all these links, as model-assessments of BB aerosol-cloud-  
108 climate interactions in the SEA critically rely on them. Constraints, however, on such links  
109 are virtually nonexistent for this region of the globe.

110 This study analyzes data collected in August 2017 on the NASA ObseRvations of  
111 Aerosols above CLouds and their intEractionS (ORACLES) campaign, and provides a  
112 systematic mapping of CCN concentration, aerosol size distribution, hygroscopicity, and  
113 cloud vertical velocity in the SEA. The in-situ measurements are then coupled with a state-  
114 of-the-art droplet parameterization to determine the in-cloud maximum supersaturation  
115 ( $S_{max}$ ) achieved in the cloud updrafts and its response to aerosol changes. The data then is  
116 used to quantify the sensitivity of droplet formation to variations in vertical velocity and  
117 aerosol. We also explore whether the presence of BB aerosol correlates with shifts in the  
118 cloud vertical velocity driving droplet formation. These perturbations in BB aerosol  
119 availability, linked with vertical updraft dynamics, and predicted cloud droplet formation  
120 allow for understanding the drivers of droplet formation in the SEA cloud deck, and the  
121 degree to which BB influences droplet formation in the boundary layer.

122

## 123 **2. Methods**

### 124 **2.1 Observational Data Set**

125 A complete description and overview of the project is provided by Redemann, et  
126 al. (in preparation). All measurements were taken aboard the National Aeronautics and  
127 Space Administration (NASA) P-3B aircraft from August 12<sup>th</sup> through 31<sup>st</sup> as part of the  
128 ORACLES 2017 campaign. The aircraft was based at the International Airport (0.3778°N,  
129 6.7131°E) of São Tomé, an island off the west coast of central Africa. A map of MODIS



130 satellite fires for the month of August 2017 can be found in Figure S1. The burning area is  
131 largely savanna grassland and the subsequent smoke plume travels westward over the SEA  
132 region. This work focuses on data collected on eight different research flights in the 2017  
133 campaign during which instrumentation providing all relevant aerosol microphysical and  
134 cloud-scale dynamics data performed optimally. Flight paths for all data used in this work  
135 can be found in Figure 1. Most flights followed a “routine” route going out to 5°E longitude  
136 and then due South. Each flight included legs at varying altitudes to capture the  
137 characteristics of the plume, the MBL, and the cloud deck. This work primarily focuses on  
138 the aerosol measured below-cloud in the MBL, as that is the aerosol that will participate in  
139 cloud droplet activation.

## 140 **2.2 Instrumentation**

141 A summary of the relevant measurements obtained at each flight can be found in  
142 Table 1. A solid diffuser inlet, characterized previously as having a 4 $\mu$ m dry diameter cut-  
143 off (McNaughton, et al. 2007), was used to sample aerosol onboard the aircraft. A Droplet  
144 Measurement Technologies (DMT; CCN-100) Continuous Flow Streamwise Thermal  
145 Gradient Chamber (CFSTGC; Roberts and Nenes, 2005) was used to measure CCN  
146 concentrations using a DMT constant pressure inlet operated at 600 mbar pressure. Since  
147 CCN measurements are highly sensitive to fluctuations in pressure and their effect on  
148 generated supersaturation (Raatikainen, et al. 2014), a flow orifice and active control  
149 system were used upstream of the instrument to ensure that the pressure remained constant,  
150 despite fluctuations in ambient pressure with altitude. The instrument was operated in both  
151 “standard” mode, where supersaturation (SS%) was stepped between 0.1, 0.2, and 0.3% by  
152 changing the temperature gradient in the droplet growth chamber, and in “scanning flow



153 CCN analysis” (SFCA) mode (Moore and Nenes, 2009), where supersaturation was varied  
154 from 0.1% to 0.4% by cycling the flow in a sinusoidal pattern from 300 to 1000 cm<sup>3</sup> min<sup>-1</sup>  
155 while maintaining a constant temperature gradient in the growth chamber. Aerosol particles  
156 that activated into droplets sized greater than 0.5µm were then counted as CCN by the  
157 optical particle counter located at the exit of the CFSTGC growth chamber.

158 A DMT Ultra High Sensitivity Aerosol Spectrometer (UHSAS) was also operated  
159 on the same 600mbar constant pressure inlet as the CFSTGC to detect the aerosol  
160 concentration from 80 to 1000 nm (Table 1). Comparison of UHSAS with DMA  
161 distributions revealed that the UHSAS counting efficiency dropped below about 80 nm  
162 (Howell et al., in preparation), which should not strongly affect our subsequent analysis –  
163 as particles larger than 80nm diameter contribute the exclusive majority of CCN that  
164 activate into droplets for the conditions considered. The aerosol size distribution was  
165 combined with CCN measurements to calculate the hygroscopicity parameter,  $\kappa$ , of the  
166 observed aerosol (Petters and Kreidenweis, 2007), following a procedure adopted in  
167 numerous studies (e.g., Kalkavouras et al., 2019; Bougiatioti et al., 2016; Moore et al.,  
168 2011; Lathem et al., 2012) where integration of the particle size distribution from the  
169 largest resolved bin in the UHSAS down to a characteristic size,  $d_{crit}$  (also known as the  
170 “critical diameter”), matches the measured CCN concentration. The hygroscopicity then is  
171 obtained from from  $d_{crit}$  and the instrument supersaturation, following Kalkavouras et al.  
172 (2019).

173 Vertical winds on the P-3B were measured with the Turbulent Air Motion  
174 Measurement System (TAMMS) (Thornhill et al., 2003). Fast-response flow-angle,  
175 pressure, and temperature sensors combined with a GPS corrected inertial navigation





176 system (INS) provide 50 Hz inputs to compute 20 Hz averaged vertical winds via the full  
177 air motion equations from Lenschow (1986). The updraft velocities are then used as an  
178 input to calculate cloud droplet number concentration via a Gaussian distribution of updraft  
179 velocities (Section 2.3).

180 An Aerodyne High-Resolution Time-of-Flight Aerosol Mass Spectrometer (HR-  
181 ToF-AMS) (Jimenez, et al., 2006) was used to monitor bulk chemical composition of  
182 sampled aerosol throughout all flights. The bulk chemical composition acquired is then  
183 used to calculate the “bulk”  $\kappa$  (Petters and Kreidenweis, 2007), based on the mass fraction  
184 of organics and sulfate in the aerosol –assuming that the hygroscopicity of the organic  
185 fraction,  $\kappa_{\text{org}}=0.1$ , and of sulfate,  $\kappa_{\text{sulfate}}=0.6$ . We have also ignored the effects of insoluble  
186 material – such as black carbon – as it constitutes a small volume fraction of the aerosol  
187 and has a negligible influence on hygroscopicity. The bulk-derived  $\kappa$  allows for comparison  
188 with the directly calculated  $\kappa$  from the CFSTGC and UHSAS measurements, even if the  
189 AMS-derived values correspond to larger sizes than the CCN-derived  $\kappa$ . Nevertheless,  
190 strong agreement is found between the two  $\kappa$  values (Table 1; Figure S1), thus confirming  
191 that the internal mixture assumption inherent to CCN-derived hygroscopicity applies, and,  
192 that the composition varies little over the size range between  $d_{\text{crit}}$  (~100-200nm) and the  
193 peak of the mass distribution resolved by the AMS. It should also be noted that all of the  
194 AMS data was in high-sensitivity mode; the AMS heater was operated at an indicated 600  
195 °C, which was tested and proved optimal for the ORACLES BBOA plume. The data were  
196 processed using the standard AMS software (Squirrel, version 1.41).

197 A Droplet Measurement Technologies (DMT) Cloud Droplet Probe (CDP) was  
198 used to measure the cloud droplet number from 2 to 50 micron in diameter. The CDP was



199 modified according to Lance et al. (2010) to reduce coincidence problems. The total cloud  
200 droplet number ( $N_d$ ) from the CDP is compared against the predicted  $N_d$  from the cloud  
201 droplet parameterization. These comparisons are done in flights with mostly stacked legs  
202 in the MBL and clouds; occasionally, flights where aerosol and cloud were immediately  
203 before or after each other were used (but not stacked).

### 204 **2.3 Predicted Cloud Droplet Number**

205 The droplet activation process is the direct microphysical link between clouds and  
206 aerosol. Every aerosol particle, to activate and form a cloud droplet, requires exposure to a  
207 “critical” supersaturation (or above) for enough time to grow past a “critical” wet size  
208 (Nenes et al., 2001) that ensures unconstrained growth. Applying this principle to ambient  
209 clouds is confounded by the complex relationship of supersaturation with aerosol size  
210 distribution, hygroscopicity, and the characteristic vertical updraft velocity. State-of-the-  
211 art cloud droplet parameterizations (e.g., Ghan et al., 2011; Morales and Nenes, 2014),  
212 however, resolve this relation and determine the cloud droplet number ( $N_d$ ), maximum  
213 available supersaturation ( $S_{max}$ ), and sensitivity of  $N_d$  to changes in aerosol concentration  
214 ( $N_a$ ), vertical updraft velocity ( $w$ ), and CCN activity ( $\kappa$ ).

215 In this study, we utilize the Nenes and Seinfeld (2003) parameterization with  
216 improvements introduced by Fountoukis and Nenes (2005), Barahona et al., (2010) and  
217 Morales and Nenes (2014). In applying the droplet parameterization, we integrate over the  
218 distribution of vertical velocities within the boundary layer – by utilizing the “characteristic  
219 vertical velocity” approach of Morales and Nenes (2010). In this approach, instead of  
220 numerically integrating over a probability density distribution (PDF), the parameterization  
221 is applied at a “characteristic” velocity,  $w^*$ , that yields the same result as the integrated



222 value over the PDF. To derive  $w^*$ , the measured vertical winds,  $w$ , are taken from all  
223 segments just below cloud in a given flight, then fit to a Gaussian distribution;  $w^*=0.79\sigma_w$ ,  
224 where  $\sigma_w$  is the width of the vertical velocity spectrum (Morales and Nenes, 2010). A  
225 consistency check of the validity of the PDF, is that the mean velocity needs to be close to  
226 zero. A comparison between the predicted  $N_d$  from the parameterization and the measured  
227  $N_d$  from the CDP can be found in Figure S2. The parameterized  $N_d$  was, on average, within  
228 20% of the measured  $N_d$ , which is within the the difference range of previous droplet  
229 closure studies (e.g., Meskhidze et al., 2005; Fountoukis et al., 2007; Morales et al., 2011).

230

### 231 **3. Results and Discussion**

#### 232 **3.1 Marine Boundary Layer Air Mass Characterization**

233 Characteristic vertical profiles of CCN concentrations from 0.1 to 0.4%  
234 supersaturation for flights used in this work are shown in Figure 2. Earlier flights (RF01 –  
235 RF03) have lower BB plume heights, relatively little vertical variation of concentration  
236 within the plume, and high CCN concentrations in the marine boundary layer (MBL). Later  
237 flights (RF08 – RF12) show distinct layering in the plume, a higher plume cap altitude, and  
238 lower MBL concentrations. Hereon we focus on aerosol concentrations in the MBL, being  
239 the relevant aerosol providing CCN for BL cloud formation. A summary of the MBL  
240 aerosol concentrations, CCN –derived  $\kappa$  (averaged over all the supersaturations measured),  
241 and characteristic vertical updraft velocity ( $w^*$ ) is provided for all flights in Table 1. Flights  
242 are classified according to the observed MBL aerosol concentrations from the UHSAS into  
243 categories defined, for the purposes of this work, as “polluted” (exceeding  $800\text{ cm}^{-3}$ ),  
244 “intermediate” ( $500\text{--}800\text{ cm}^{-3}$ ), and “clean” (below  $500\text{ cm}^{-3}$ ). MBL aerosol concentration



245 is higher earlier on in August and decreases as the mission progresses. The average CCN-  
246 derived  $\kappa$  for the MBL aerosol is fairly consistent, ranging from 0.2 to 0.4, and agrees well  
247 with the  $\kappa$  estimated from the bulk MBL aerosol elemental composition as measured by  
248 the aerosol mass spectrometer, implying that the aerosol is chemically uniform throughout  
249 the ultrafine aerosol size range (Figure S1).

250 Characteristic vertical updrafts are higher earlier in August, averaging  $0.4 \text{ ms}^{-1}$ , and  
251 decrease to around  $0.3 \text{ ms}^{-1}$  later in the campaign. A decrease in MBL aerosol concentration  
252 is also seen during this time, with earlier flights seeing aerosol concentrations reaching up  
253 to  $1000 \text{ cm}^{-3}$  and later decreasing to  $200 \text{ cm}^{-3}$ . The average BB plume aerosol  
254 concentrations aloft range from around  $1250 \text{ cm}^{-3}$  to  $3000 \text{ cm}^{-3}$ , but show no distinct trends  
255 throughout the month. However, an interesting trend can be found in comparing the  
256 altitudes of the bottom of the BB plume and the top of the MBL cloud deck with the  
257 characteristic vertical updraft velocities – a lower  $w^*$  of  $0.3 \text{ ms}^{-1}$  coincides with observation  
258 of a clean, low-aerosol “gap” between the top of the MBL clouds and the bottom of the BB  
259 plume. In higher  $w^*$  flights ( $0.4 \text{ ms}^{-1}$ ), the BB plume extends all the way down to the top  
260 of the MBL cloud layers. In these flights, the BB plume is observed to have one single,  
261 well-mixed layer throughout, while the later flights ( $w^* \sim 0.3 \text{ ms}^{-1}$ ) are characterized by  
262 two distinct layers in the plume.

263

### 264 **3.2 Predicted Droplet Number and Maximum Supersaturation**

265 Figure 3a presents predicted droplet number ( $N_d$ ) and CCN (at 0.1%  
266 supersaturation) as a function of total aerosol concentration ( $N_a$ ) for the marine boundary  
267 layer (MBL) legs of all flights. Above an aerosol concentration of  $\sim 600 \text{ cm}^{-3}$ , droplet



268 number concentration becomes progressively less responsive to further increases in CCN  
269 number (as the incremental change in  $N_d$  is less as CCN increases) and becomes effectively  
270 insensitive ( $\partial N_d / \partial N_a \sim 0$ ) for an aerosol concentration exceeding  $\sim 1000 \text{ cm}^{-3}$ . The reason  
271 behind this increasing insensitivity can be seen in Figure 3b, which presents  $N_d$  against  $N_a$   
272 for all the MBL leg data; the data are colored by supersaturation. For low values of  $N_a$  and  
273  $N_d$  ( $\sim 200 \text{ cm}^{-3}$ ),  $S_{max}$  tends to be high (just over 0.2%) and the response of  $N_d$  to increases  
274 in aerosol is strong. However, when transitioning from “clean” to “intermediate” MBL  
275 conditions,  $N_d$  is less sensitive to increases in aerosol, because  $S_{max}$  decreases, and mitigates  
276 some of the expected droplet number response. Upon reaching “polluted” conditions ( $\sim 900$   
277  $\text{cm}^{-3}$ ), the decrease in  $S_{max}$  is even stronger, entering into a regime where any additional  
278 aerosol can no longer substantially augment cloud droplets, owing to the extreme  
279 competition of the high CCN concentrations for water vapor. This water vapor-limited  
280 regime occurs when the  $S_{max}$  is less than 0.1% (Figure 3b); given that water vapor  
281 availability is generated through expansion cooling in updrafts, this type of limitation is  
282 also known as the “updraft-limited” regime of droplet formation (Ruetter et al., 2009).

283

### 284 3.3 Droplet Number Sensitivity

285 The previous section pointed out the variable sensitivity of droplet number to  
286 aerosol perturbations, depending on the conditions of cloud formation. To further explore  
287 such issues, we explicitly calculate the sensitivities (partial derivatives) of droplet number  
288 in the MBL to changes in aerosol number, characteristic vertical updraft velocity, and CCN  
289 activity, computed by the parameterization using a finite difference approximation. This is  
290 shown in Figure 4 for  $\partial N_d / \partial N_a$  (top panel),  $\partial N_d / \partial w$  (middle panel) and  $\partial N_d / \partial \kappa$  (bottom



291 panel). Results are shown for three flights, corresponding to each pollution class of Table  
292 1: “polluted” (RF02), “intermediate” (RF09), and “clean” (RF10). Sensitivity of droplet  
293 number to total aerosol concentration ( $\partial N_d/\partial N_a$ ) is fairly comparable between the two lower  
294 concentration conditions and approaches insensitivity ( $\partial N_d/\partial N_a < 0.1$ ) when the total  
295 aerosol concentration exceeds  $1000 \text{ cm}^{-3}$ . Maximum in-cloud supersaturation decreases  
296 steadily as  $N_a$  increases and  $\partial N_d/\partial N_a$  appreciably decreases when  $S_{max}$  drops below 0.12%  
297 (Figure 4, top panel).

298 As  $\partial N_d/\partial N_a$  decreases with increasing levels of aerosol, droplet sensitivity to  
299 vertical updraft velocity,  $\partial N_d/\partial w$ , becomes increasingly important and completely  
300 dominates droplet variability for high aerosol numbers. The reason why droplets become  
301 so sensitive to vertical velocity fluctuations under polluted conditions, is because vertical  
302 velocity drives supersaturation generation; at low supersaturation, when there is very  
303 strong competition for water vapor from the many CCN present (“velocity-limited  
304 regime”), any increase in vertical velocity augments supersaturation and droplet number.  
305 For low CCN concentrations, however, supersaturation is high so that fluctuations in  
306 aerosol translate to an almost equal response in droplet number ( $\partial N_d/\partial N_a \sim 1$ ; Figure 4,  
307 top panel), therefore fluctuations in vertical velocity, hence supersaturation, do not affect  
308 droplet number ( $\partial N_d/\partial w$  small). The low MBL aerosol concentrations lead to the highest  
309 sensitivity of  $N_d$  to  $N_a$  (approaching 100%), creating an “aerosol-limited” condition where  
310 there is sufficient available supersaturation to activate virtually every aerosol added to the  
311 MBL layer. A  $\sim 5x$  increase in  $N_a$  leads to a  $\sim 50\%$  decrease in the sensitivity of  $N_d$  to  $N_a$  to  
312 around 40%, with the highest aerosol values corresponding to even lower sensitivities to



313 aerosol number, approaching below 10% and clearly behavior consistent with a “velocity-  
314 limited” regime.

315 Predicted droplet sensitivity to  $\kappa$  displays a unique trend (Figure 4, bottom panel),  
316 becoming stronger initially with increasing aerosol, peaking at intermediate concentrations  
317 and then rapidly dropping towards insensitivity, when supersaturation approaches 0.1%.  
318 This sudden insensitivity to CCN activity aligns with the clouds being overseeded when  
319 supersaturation is starting to be depleted – once supersaturation is not as readily available,  
320 any characteristics of the aerosol cease to play a strong role in activation. However, prior  
321 to reaching the point of being insensitive to aerosol, increased sensitivity to  $\kappa$  is opposite  
322 to the expected trend from  $N_a$  – indicating that the fluctuation in chemical composition,  
323 when droplet formation is in a “competitive” regime (Figure 4c), may be an important  
324 contributor to droplet formation – consistent with the findings of Bougiatioti et al., (2017)  
325 for droplet formation in an urban environment in the E.Mediterranean. We emphasize here  
326 that the sensitivity to  $\kappa$  (Figure 4c) is not from its changes over size (which we show above  
327 to be small), but rather changes over space and time.

328

### 329 **3.2.1 Impact of Boundary Layer Turbulence**

330 Throughout the entirety of flights, the maximum predicted droplet number reaches  
331 a plateau, where additional aerosol does not result in any significant increase in  $N_d$ . An  
332 example of this behavior is presented in Supplementary Figure S4 (where data of calculated  
333  $N_d$  is presented for the entire research flight, as opposed to only the segments in the MBL  
334 shown in previous sections). This plateau, owing to the development of strong water vapor  
335 limitations, is termed limiting droplet number,  $N_d^{lim}$ , and should largely be a function of



336 vertical velocity – precisely because we are in a velocity-limited regime. This realization  
337 implies that much of the droplet number variability (measured or retrieved) in clouds  
338 strongly influenced by BB plumes reflects the underlying shifts in cloud dynamics  
339 associated with each concentration “regime”. Indeed, the characteristic velocity in the  
340 MBL tends to increase as the MBL clouds become progressively polluted (Figure 5); the  
341 higher pollution flights (RF01 and RF02) all fall in mid-August and are coincident with a  
342 higher characteristic vertical updraft velocity of  $\sim 0.4$ , while “clean” MBL flights coincide  
343 with lower vertical updraft velocity values of  $\sim 0.3$  and occur towards the end of August.  
344 “Intermediate” scenario flights are divided between the two characteristic vertical updraft  
345 velocities observed. When the flight-specific characteristic velocity is then used to  
346 calculate the droplet response, it follows a trend with aerosol levels that magnifies droplet  
347 response from what is expected by increasingly adding pollution alone. In contrast, the  
348 aerosol concentration above the MBL is inversely correlated with  $w^*$  (Figure 5), possibly  
349 a result of enhanced mixing between the MBL and the free troposphere (rich in BB aerosol)  
350 that is associated with the elevated levels of turbulence ( $w^*$ ).

351 The impact of increased  $w^*$  on the droplet number is shown for “polluted”,  
352 “intermediate” and “clean” conditions in the inset plot of Figure 5 – which shows  $N_d^{lim}$  for  
353 each concentration class for  $w^*$  between  $0.1$  and  $0.6 \text{ ms}^{-1}$ . For polluted conditions,  
354 transitioning from  $0.3$  to  $0.4 \text{ ms}^{-1}$  increases droplet number from  $400$  to  $500 \text{ cm}^{-3}$ , which is  
355 a 20-25% increase. The enhancement is equally important for intermediate and clean  
356 conditions (although less in absolute number), and always comparable to droplet  
357 enhancements from changes in BB concentration.

358





359 **3.4 Water-vapor limitations and the lifetime of BB aerosol in the MBL**

360 Above an aerosol concentration of  $\sim 800 \text{ cm}^{-3}$  when water vapor availability is  
361 severely limited,  $N_d$  no longer increases in response to increases in CCN (Figure 3a). An  
362 important consequence is that under such conditions, much of the BBOA does not activate  
363 into cloud droplets and is therefore not lost through wet deposition. Because of this, the  
364 degree of water vapor competition (and supersaturation level) is directly related to BB  
365 lifetime in the MBL (Figure 9).  $\partial N_d / \partial d N_a$  may then be inversely linked to CCN lifetime,  
366 where “velocity-limited” conditions, characterized by the smallest droplet activation  
367 fraction and  $\partial N_d / \partial d N_a$ , also have the largest lifetime and vice versa for “clean” MBL  
368 conditions.

369

370 **4. Implications and Conclusions**

371 BB aerosol levels in the SEA varied considerably throughout the 2017 ORACLES  
372 deployment. Earlier in the campaign, high aerosol concentrations were observed in the  
373 MBL ( $800\text{-}1000 \text{ cm}^{-3}$ ), which decreased mid-campaign to concentrations between  $500\text{-}800$   
374  $\text{cm}^{-3}$ , and in late August and early September, relatively clean MBL conditions were seen  
375 ( $<500 \text{ cm}^{-3}$ ). On 12-13 August, MBL aerosol concentrations exceeded  $1000 \text{ cm}^{-3}$ . From the  
376 observed aerosol size distribution and CCN concentrations, we constrained the aerosol  
377 hygroscopicity – which was in agreement with estimates from bulk chemical composition  
378 measurements; together with observed MBL vertical velocity distributions, we then  
379 calculate droplet number concentrations using a state-of-the-art droplet activation  
380 parameterization. Droplet closure was achieved within 20%, consistent with the degree of  
381 closure achieved in past studies.



382 From the analysis of the dataset, when aerosol concentrations exceed  $\sim 900 \text{ cm}^{-3}$   
383 and maximum supersaturation approaches 0.1%, droplet formation in the MBL begins to  
384 enter a “velocity-limited” droplet activation regime, where cloud droplet number responds  
385 weakly to CCN concentration increases. Lower MBL concentrations ( $500 \text{ cm}^{-3}$  or less)  
386 were observed later in the campaign (late August to early September), thus leading to a  
387 much higher predicted  $S_{max}$  of 0.2%, and much higher fraction of activated CCN. Under  
388 clean conditions, vertical velocity generates ample supersaturation, so droplet formation is  
389 limited by the number of aerosol particles in the MBL. Overall this leads to a buffering of  
390 the  $N_d$  response to aerosol, so that  $N_d$  variability is much less (down to 1/10 or less) than  
391 that seen for the underlying CCN.

392 Droplet formation sensitivity to aerosol concentration, vertical updraft velocity, and  
393 the hygroscopicity parameter,  $\kappa$ , vary and contribute to the total droplet response in the  
394 MBL clouds. Droplet sensitivity to vertical velocity increases an order of magnitude as  
395 aerosol concentration reaches  $1000 \text{ cm}^{-3}$ . This highlights the increased (and eventually  
396 dominant) role that vertical velocity plays in droplet formation in a “polluted” MBL  
397 environment. Below  $\sim 500 \text{ cm}^{-3}$ , in a “clean” MBL, droplet formation is much more  
398 sensitive to changes in aerosol concentration than to the observed changes in vertical  
399 updrafts. In the “competitive” regime, where the MBL has “intermediate” pollution (500-  
400  $800 \text{ cm}^{-3}$ ), hygroscopicity ( $\kappa$ ) variations emerges as an important driver of droplet number  
401 variability, which is something not seen for either “clean” or “polluted” MBL conditions.  
402 Throughout the month of August, a shift is observed in  $w^*$ , from  $\sim 0.45 \text{ m s}^{-1}$  down to  $\sim 0.26$   
403  $\text{m s}^{-1}$ , which affects the maximum droplet number that can be generated in the MBL.  $N_d^{lim}$   
404 is significantly affected by changes in  $w^*$ , especially in higher MBL pollution conditions,



405 where the effects of increased characteristic vertical updraft velocity significantly  
406 magnifies droplet number concentrations compared to trends seen in “intermediate” and  
407 “clean” MBL environments.

408 Identifying regimes where droplet number variability is primarily driven by updraft  
409 velocity changes, and not aerosol concentration, is key for interpreting aerosol indirect  
410 effects. This is particularly important when using remote sensing data, as can be seen from  
411 the data here: diagnosing aerosol indirect effects using above-cloud aerosol would give  
412 opposite trends from what actually occurs in the MBL – because BB plume aerosol  
413 decreases as the MBL aerosol increases. Nevertheless, the correlations here between  
414 above-cloud and MBL aerosol level might be a useful way to diagnose MBL aerosol –  
415 from which  $N_d$  can eventually be determined. Furthermore, when droplet number is in the  
416 velocity-limited regime,  $N_d$  responds proportionally to changes in  $w^*$ , offering the  
417 possibility of remote sensing of  $w^*$  under these specific conditions (specific criteria need  
418 to be developed to help define when velocity-limited conditions occur, e.g., combining  
419 collocated in-situ and remote sensing data from field intensives).

420 Very interesting are the trends observed between MBL dynamics, height and the  
421 aerosol levels in the MBL and the BB plume.  $w^*$  is higher earlier in August and decreases  
422 later in the campaign; MBL aerosol concentration correlates with  $w^*$ , while an inverse  
423 correlation is seen for the aerosol in the BB plume above the MBL. A similarly interesting  
424 trend can be found between  $w^*$ , the base altitude of the BB plume and the top of the MBL  
425 cloud deck: higher  $w^*$  corresponds to a BB plume that extends down to the top of the MBL  
426 cloud layers, while lower  $w^*$  is characterized by two distinct layers in the plume. Although  
427 what drives these correlations is not fully understood, it is likely related to the seasonality



428 of the MBL height and its role in regulating mixing between the MBL and aloft (also  
429 discussed in Zhang et al., 2018). Indeed, the atmosphere is likely less stable in August,  
430 encouraging buoyant parcels (hence larger  $w^*$ ) than in September.  $w^*$  enhancement may  
431 also result from enhanced cloud-top radiative cooling driven by LWC changes between the  
432 early and later flights of the campaign –the nearly threefold increase in cloud droplet  
433 number and the expected LWC response, however, suggests that clouds may actually be  
434 thinner (Painemal and Zuidema, 2010; Wood et al., 2012; de Szoeko et al., 2018).  
435 Absorption of solar radiation from black carbon in the MBL may also suppress turbulence  
436 and  $w^*$  (Wilcox et al., 2016), although our data suggests these effects may not be strong  
437 enough to reverse the trend imposed by any MBL seasonality. A thorough attribution of  
438 the link between  $w^*$ , aerosol, MBL structure and the large scale remains to be carried out.

439         Although BB aerosol variations can profoundly impact cloud microphysical  
440 characteristics, concurrent variations in vertical velocity must also be considered to fully  
441 understand the drivers of droplet variability, especially when used to evaluate models and  
442 estimates of aerosol-cloud-climate interactions. The small activation fraction of aerosols  
443 under polluted MBL conditions may promote the persistence of aerosol for longer in the  
444 MBL, extending the reach and influence of BB aerosol in the SEA.

445

446



447 **Acknowledgements**

448 MK and TN gratefully acknowledge funding from NASA ORACLES grant  
449 NNX15AL68G and the European Research Council, CoG-2016 project PyroTRACH  
450 (726165) funded by H2020-EU.1.1. – Excellent Science. All other authors acknowledge  
451 support from the NASA EVS-2 program for their individual ORACLES grants. All  
452 ORACLES datasets are publicly available through doi:  
453 10.5067/Suborbital/ORACLES/P3/2017\_V1

454 **Code/Data availability**

455 The droplet parameterization used for the calculations in the study is available from the  
456 [athanasios.nenes@epfl.ch](mailto:athanasios.nenes@epfl.ch) upon request

457 **Author contribution**

458 conceptualization, M.K. and A.N.; methodology, M.K. and A.N.; software, A.N.; formal  
459 analysis, M.K., A.N., S.H.; investigation, A.B. and A.N.; writing—original draft  
460 preparation, M.K. and A.N.; writing—review and editing: all authors.

461 **Competing interests**

462 The authors declare no competing interests.  
463



## 464 References

- 465 Adebisi, A. A., and Zuidema, P.: The role of the southern African easterly jet in modifying  
466 the southeast Atlantic aerosol and cloud environments, *Q.J.R. Meteorol. Soc.*, 142, 1574-  
467 1589. doi:10.1002/qj.2765, 2016.
- 468 Albrecht, B. A.: Aerosols, Cloud Microphysics, and Fractional Cloudiness, *Science*, 245,  
469 4923, 1227-1230, doi:10.1126/science.245.4923.1227, 1989.
- 470 Andela, N., Morton, D. C., Giglio, L., Chen, Y., van der Werf, G. R., Kasibhatla, P. S.,  
471 DeFries, R. S., Collatz, G. J., Hantson, S., Kloster, S., Bachelet, D., Forrest, M., Lasslop,  
472 G., Li, F., Mangeon, S., Melton, J. R., Yue, C., Randerson, J. T.: A human-driven decline  
473 in global burned area, *Science*, 356, 6345, 1356-1362, doi: 10.1126/science.aal4108, 2017.
- 474 Barahona, D., West, R. E. L., Stier, P., Romakkaniemi, S., Kokkola, H., and Nenes, A.:  
475 Comprehensively accounting for the effect of giant CCN in cloud activation  
476 parameterizations, *Atmos. Chem. Phys.*, 10, 2467-2473, [https://doi.org/10.5194/acp-10-](https://doi.org/10.5194/acp-10-2467-2010)  
477 2467-2010, 2010.
- 478 Bond et al 2013 Bond, T. C., Doherty, S. J., Fahey, D. W., Forster, P. M., Berntsen, T.,  
479 DeAngelo, B. J., Flanner, M. G., Ghan, S., Kärcher, B., Koch, D., Kinne, S., Kondo, Y.,  
480 Quinn, P. K., Sarofim, M. C., Schultz, M. G., Schulz, M., Venkataraman, C., Zhang, H.,  
481 Zhang, S., Bellouin, N., Guttikunda, S. K., Hopke, P. K., Jacobson, M. Z., Kaiser, J. W.,  
482 Klimont, Z., Lohmann, U., Schwarz, J. P., Shindell, D., Storelvmo, T., Warren, S. G.,  
483 Zender, C. S.: Bounding the role of black carbon in the climate system: A scientific  
484 assessment, *J. Geophys. Res.*, 118, 5380– 5552, doi:10.1002/jgrd.50171, 2013.
- 485 Boucher, O., Randall, D., Artaxo, P., Bretherton, C., Feingold, G., Forster, P., Kerminen,  
486 V.-M., Kondo, Y., Liao, H., Lohmann, U., Rasch, P., Satheesh, S. K., Sherwood, S.,  
487 Stevens, B., and Zhang, X. Y.: Clouds and aerosols. In *Climate Change 2013: The Physical  
488 Science Basis. Contribution of Working Group I to the Fifth Assessment Report of the  
489 Intergovernmental Panel on Climate Change*. T.F. Stocker, D. Qin, G.-K. Plattner, M.  
490 Tignor, S.K. Allen, J. Doschung, A. Nauels, Y. Xia, V. Bex, and P.M. Midgley, Eds.  
491 Cambridge University Press, pp. 571-657, doi:10.1017/CBO9781107415324.016.
- 492 Bougiatioti, A., Bezantakos, S., Stavroulas, I., Kalivitis, N., Kokkalis, P., Biskos, G.,  
493 Mihalopoulos, N., Papayannis, A., and Nenes, A.: Biomass-burning impact on CCN  
494 number, hygroscopicity and cloud formation during summertime in the eastern  
495 Mediterranean, *Atmos. Chem. Phys.*, 16, 7389-7409, doi:10.5194/acp-16-7389-2016, 2016.
- 496 Bougiatioti, A., Argyrouli, A., Solomos, S., Vratolis, S., Eleftheriadis, K., Papayannis, A.,  
497 and Nenes, A.: CCN Activity, Variability and Influence on Droplet Formation during the  
498 HygrA-Cd Campaign in Athens. *Atmosphere*, 8, 108, 2017.
- 499 Cubison, M. J., Ervens, B., Feingold, G., Docherty, K. S., Ulbrich, I. M., Shields, L.,  
500 Prather, K., Hering, S., and Jimenez, J. L.: The influence of chemical composition and  
501 mixing state of Los Angeles urban aerosol on CCN number and cloud properties, *Atmos.  
502 Chem. Phys.*, 8, 5649-5667, doi:10.5194/acp-8-5649-2008, 2008.



- 503 de Szoeké, S. P., Verlinden, K. L., and Covert, D.: Cloud-scale droplet number sensitivity  
504 to liquid water path in marine stratocumulus. *J. Geoph. Res.*, 123, 5320–5334, doi:  
505 10.1029/2017JD027508, 2018.
- 506 Dusek, U., Frank, G. P., Hildebrandt, L., Curtius, J., Schneider, J., Walter, S., Chand, D.,  
507 Drewnick, F., Hings, S., Jung, D., Borrmann, S., and Andreae, M. O.: Size Matters More  
508 Than Chemistry for Cloud-Nucleating Ability of Aerosol Particles, *Science*, 312:578,  
509 1375-1378, 2006.
- 510 Fanourgakis, G. S., Kanakidou, M., Nenes, A., Bauer, S. E., Bergman, T., Carslaw, K. S.,  
511 Grini, A., Hamilton, D. S., Johnson, J. S., Karydis, V. A., Kirkevåg, A., Kodros, J. K.,  
512 Lohmann, U., Luo, G., Makkonen, R., Matsui, H., Neubauer, D., Pierce, J. R., Schmale, J.,  
513 Stier, P., Tsigaridis, K., van Noije, T., Wang, H., Watson-Parris, D., Westervelt, D. M.,  
514 Yang, Y., Yoshioka, M., Daskalakis, N., Decesari, S., Gysel-Beer, M., Kalivitis, N., Liu,  
515 X., Mahowald, N. M., Myriokefalitakis, S., Schrödner, R., Sfakianaki, M., Tsimpidi, A. P.,  
516 Wu, M., and Yu, F.: Evaluation of global simulations of aerosol particle and cloud  
517 condensation nuclei number, with implications for cloud droplet formation, *Atmos. Chem.*  
518 *Phys.*, 19, 8591-8617, <https://doi.org/10.5194/acp-19-8591-2019>, 2019.
- 519 Fountoukis, C., and Nenes, A.: Continued development of a cloud droplet formation  
520 parameterization for global climate models, *J. Geophys. Res.*, 110, D11212,  
521 doi:10.1029/2004JD005591, 2005.
- 522 Fountoukis, C., Nenes, A., Meskhidze, N., Bahreini, R., Brechtel, F., Conant, W. C.,  
523 Jonsson, H., Murphy, S., Sorooshian, A., Varutbangkul, V., R. C. Flagan, and J. H.  
524 Seinfeld: Aerosol–cloud drop concentration closure for clouds sampled during ICARTT,  
525 *J. Geoph. Res.*, **112**, D10S30, doi:10.1029/2006JD007272, 2007.
- 526 Garstang, M., Tyson, P. D., Swap, R., Edwards, M., Källberg, P., and Lindesay, J. A.:  
527 Horizontal and vertical transport of air over southern Africa, *J. Geophys. Res.*, 101(D19),  
528 23721– 23736, doi:10.1029/95JD00844, 1996.
- 529 Ghan, S. J., Abdul-Razzak, H., Nenes, A., Ming, Y., Liu, X., Ovchinnikov, M., Shipway,  
530 B., Meskhidze, N., Xu, J., and Shi, X.: Droplet nucleation: Physically-based  
531 parameterizations and comparative evaluation, *J. Adv. Model. Earth Syst.*, 3, M10001,  
532 doi:10.1029/2011MS000074, 2011.
- 533 Grosvenor, D. P., Sourdeval, O., Zuidema, P., Ackerman, A., Alexandrov, M. D., Bennartz,  
534 R., et al.: Remote sensing of droplet number concentration in warm clouds: A review of the  
535 current state of knowledge and perspectives, *Rev. Geoph.*, 56, 409–453,  
536 doi:10.1029/2017RG000593, 2018.
- 537 IPCC, 2013: Climate Change 2013: The Physical Science Basis. Contribution of Working  
538 Group I to the Fifth Assessment Report of the Intergovernmental Panel on Climate Change  
539 [Stocker, T.F., D. Qin, G.-K. Plattner, M. Tignor, S.K. Allen, J. Boschung, A. Nauels, Y.  
540 Xia, V. Bex and P.M. Midgley (eds.)]. Cambridge University Press, Cambridge, United  
541 Kingdom and New York, NY, USA, 1535 pp, doi:10.1017/CBO9781107415324.



- 542 DeCarlo, P.F., J.R. Kimmel, A. Trimborn, M.J. Northway, J.T. Jayne, A.C. Aiken, M.  
543 Gonin, K. Fuhrer, T. Horvath, K. Docherty, D.R. Worsnop, and J.L. Jimenez: Field-  
544 Deployable, High-Resolution, Time-of-Flight Aerosol Mass Spectrometer, *Analytical*  
545 *Chemistry*, 78: 8281-8289, 2006.
- 546 Kalkavouras, P., Bougiatioti, A., Kalivitis, N., Tombrou, M., Nenes, A., and Mihalopoulos,  
547 N.: Regional New Particle Formation as Modulators of Cloud Condensation Nuclei and  
548 Cloud Droplet Number in the Eastern Mediterranean, *Atmos. Chem. Phys.*, **19**, 6185-6203,  
549 <https://doi.org/10.5194/acp-19-6185-2019>, 2019
- 550 Kanakidou, M., Seinfeld, J. H., Pandis, S. N., Barnes, I., Dentener, F. J., Facchini, M. C.,  
551 Van Dingenen, R., Ervens, B., Nenes, A., Nielsen, C. J., Swietlicki, E., Putaud, J. P.,  
552 Balkanski, Y., Fuzzi, S., Horth, J., Moortgat, G. K., Winterhalter, R., Myhre, C. E. L.,  
553 Tsigaridis, K., Vignati, E., Stephanou, E. G., and Wilson, J.: Organic aerosol and global  
554 climate modelling: a review, *Atmos. Chem. Phys.*, 5, 1053-1123, doi:10.5194/acp-5-1053-  
555 2005, 2005.
- 556 Kerminen, V.-M., Paramonov, M., Anttila, T., Riipinen, I., Fountoukis, C., Korhonen, H.,  
557 Asmi, E., Laakso, L., Lihavainen, H., Swietlicki, E., Svenningsson, B., Asmi, A., Pandis,  
558 S. N., Kulmala, M., and Petäjä, T.: Cloud condensation nuclei production associated with  
559 atmospheric nucleation: a synthesis based on existing literature and new results, *Atmos.*  
560 *Chem. Phys.*, 12, 12037-12059, doi:10.5194/acp-12-12037-2012, 2012.
- 561 Klein, S. A., and Hartmann, D. L.: The Seasonal Cycle of Low Stratiform Clouds. *J.*  
562 *Climate*, 6, 1587–1606, doi:10.1175/1520-0442(1993)006<1587:TSCOLS>2.0.CO;2,  
563 1993.
- 564 Kohler, H.: The nucleus in and the growth of hygroscopic droplets, *Trans Farad Soc*, 32,  
565 1152–1161, 1936.
- 566 Lance, S., Brock, C. A., Rogers, D., and Gordon, J. A.: Water droplet calibration of the  
567 Cloud Droplet Probe (CDP) and in-flight performance in liquid, ice and mixed-phase  
568 clouds during ARCPAC, *Atmos. Meas. Tech.*, 3, 1683–1706, [https://doi.org/10.5194/amt-](https://doi.org/10.5194/amt-3-1683-2010)  
569 [3-1683-2010](https://doi.org/10.5194/amt-3-1683-2010), 2010.
- 570 Latham, T.L., A.J. Beyersdorf, K.L. Thornhill, E.L. Winstead, M.J. Cubison, A. Hecobian,  
571 J.L. Jimenez, R.J. Weber, B.E. Anderson, and Nenes, A.: Analysis of CCN activity of  
572 Arctic aerosol and Canadian biomass burning during summer 2008, *Atmos.Chem.Phys.*,  
573 **13**, 2735-2756, 2013.
- 574 Lenschow, D.H., ed. 1986: *Probing the Atmospheric Boundary Layer*. Amer. Meteorol.  
575 Soc
- 576 McNaughton, C. S., Clarke, A. D., Howell, S. G., Pinkerton, M., Anderson, B., Thornhill,  
577 L., Hudgins, C., Winstead, E., Dibb, J. E., Scheuer, E., and Maring, H.: Results from the  
578 DC-8 Inlet Characterization Experiment (DICE): Airborne Versus Surface Sampling of  
579 Mineral Dust and Sea Salt Aerosols, *Aero. Sci. Tech.*, 41:2, 136-159,  
580 doi:10.1080/02786820601118406, 2007.





- 581 Meskhidze, N., A. Nenes, Conant, W. C., and Seinfeld, J.H.: Evaluation of a new Cloud  
582 Droplet Activation Parameterization with In Situ Data from CRYSTAL-FACE and  
583 CSTRIFE, *J. Geoph. Res.*, **110**, D16202, doi:10.1029/2004JD005703, 2005.
- 584 Moore, R. H., and Nenes, A.: Scanning Flow CCN Analysis—A Method for Fast  
585 Measurements of CCN Spectra, *Aero. Sci. Tech.*, 43:12, 1192-1207,  
586 doi:10.1080/02786820903289780, 2009.
- 587 Moore, R.H., Bahreini, R., Brock, C.A., Froyd, K.D., Cozic, J., Holloway, J.S.,  
588 Middlebrook, A.M., Murphy, D.M., Nenes, A.: Hygroscopicity and Composition of  
589 Alaskan Arctic CCN During April 2008, *Atmos. Chem. Phys.*, **11**, 11807-11825, 2011.
- 590 Morales, R., and Nenes, A.: Characteristic updrafts for computing distribution-averaged  
591 cloud droplet number and stratocumulus cloud properties, *J. Geophys. Res.*, 115, D18220,  
592 doi:10.1029/2009JD013233, 2010.
- 593 Morales Betancourt, R. and Nenes, A.: Understanding the contributions of aerosol  
594 properties and parameterization discrepancies to droplet number variability in a global  
595 climate model, *Atmos. Chem. Phys.*, 14, 4809-4826, doi:10.5194/acp-14-4809-2014, 2014.
- 596 Morales, R., Nenes, A., Jonsson, H., Flagan, R.C. and J.H. Seinfeld: Evaluation of a  
597 diabatic droplet activation parameterization using in-situ cloud data, *J. Geoph. Res.*, **116**,  
598 D15205, doi:10.1029/2010JD015324, 2011.
- 599 Myhre, G., Samset, B. H., Schulz, M., Balkanski, Y., Bauer, S., Berntsen, T. K., Bian, H.,  
600 Bellouin, N., Chin, M., Diehl, T., Easter, R. C., Feichter, J., Ghan, S. J., Hauglustaine, D.,  
601 Iversen, T., Kinne, S., Kirkevåg, A., Lamarque, J.-F., Lin, G., Liu, X., Lund, M. T., Luo,  
602 G., Ma, X., van Noije, T., Penner, J. E., Rasch, P. J., Ruiz, A., Seland, Ø., Skeie, R. B.,  
603 Stier, P., Takemura, T., Tsigaridis, K., Wang, P., Wang, Z., Xu, L., Yu, H., Yu, F., Yoon,  
604 J.-H., Zhang, K., Zhang, H., and Zhou, C.: Radiative forcing of the direct aerosol effect  
605 from AeroCom Phase II simulations, *Atmos. Chem. Phys.*, 13, 1853-1877,  
606 doi:10.5194/acp-13-1853-2013, 2013.
- 607 Nenes, A., Ghan, S., Abdul-Razzak, H., Chuang, P.Y., Seinfeld, J.H.: Kinetic Limitations  
608 on Cloud Droplet Formation and Impact on Cloud Albedo, *Tellus*, 53B, 133-149, 2001
- 609 Nenes, A., and Seinfeld, J. H.: Parameterization of cloud droplet formation in global  
610 climate models, *J. Geophys. Res.*, 108, 4415, doi:10.1029/2002JD002911, D14, 2003.
- 611 Petters, M. D. and Kreidenweis, S. M.: A single parameter representation of hygroscopic  
612 growth and cloud condensation nucleus activity, *Atmos. Chem. Phys.*, 7, 1961-1971,  
613 doi:10.5194/acp-7-1961-2007, 2007.
- 614 Petters, M. D. and Kreidenweis, S. M.: A single parameter representation of hygroscopic  
615 growth and cloud condensation nucleus activity – Part 2: Including solubility, *Atmos.*  
616 *Chem. Phys.*, 8, 6273-6279, doi:10.5194/acp-8-6273-2008, 2008.



- 617 Pósfai, M., Simonics, R., Li, J., Hobbs, P. V., and Busek, P. R.: Individual aerosol particles  
618 from biomass burning in southern Africa: 1. Compositions and size distributions of  
619 carbonaceous particles, *J. Geophys. Res.*, 108, 8483, doi:10.1029/2002JD002291, D13,  
620 2003.
- 621 Raatikainen, T., Lin, J. J., Cerully, K. M., Latham, T. L., Moore, R. H., and Nenes, A.:  
622 CCN Data Interpretation Under Dynamic Operation Conditions, *Aero. Sci. Tech.*, 48:5,  
623 552-561, doi:10.1080/02786826.2014.899429, 2014.
- 624 Raatikainen, T., Nenes, A., Seinfeld, J. H., Morales, R., Moore, R. H., Latham, T. L., Lance,  
625 S., Padro, L. T., Lin, J. J., Cerully, K., Bougiatioti, A., Cozic, J., Ruehl, C., Chuang, P. Y.,  
626 Anderson, B., Flagan, R. C., Jonsson, H., Mihalopoulos, N., and J. N. Smith: Worldwide  
627 data sets constrain the water vapor uptake coefficient in cloud formation,  
628 *Proc. Nat. Acad. Sci.*, doi: 10.1073/pnas.1219591110, 2013
- 629 Redemann, J., et al.: An overview of the ORACLES (ObseRvations of Aerosols above  
630 CLouds and their intERactionS) project: aerosol-cloud-radiation interactions in the  
631 Southeast Atlantic basin, in preparation.
- 632 Rissman, T., Nenes, A., and Seinfeld, J. H.: Chemical amplification (or dampening) of the  
633 Twomey effect: Conditions derived from droplet activation theory, *J. Atmos. Sci.*, 61, 919–  
634 930, 2004.
- 635 Reutter, P., Su, H., Trentmann, J., Simmel, M., Rose, D., Gunthe, S. S., Wernli, H.,  
636 Andreae, M. O., and Pöschl, U.: Aerosol- and updraft-limited regimes of cloud droplet  
637 formation: influence of particle number, size and hygroscopicity on the activation of cloud  
638 condensation nuclei (CCN), *Atmos. Chem. Phys.*, 9, 7067-7080,  
639 <https://doi.org/10.5194/acp-9-7067-2009>, 2009
- 640 Roberts, G. C., and Nenes, A.: A Continuous-Flow Streamwise Thermal-Gradient CCN  
641 Chamber for Atmospheric Measurements, *Aero. Sci. Tech.*, 39:3, 206-221,  
642 doi:10.1080/027868290913988, 2005.
- 643 Ross, K. E., Piketh, S. J., Bruintjes, R. T., Burger, R. P., Swap, R. J., and Annegarn, H. J.:  
644 Spatial and seasonal variations in CCN distribution and the aerosol-CCN relationship over  
645 southern Africa, *J. Geophys. Res.*, 108, 8481, doi:10.1029/2002JD002384, D13, 2003.
- 646 Seager, R., Murtugudde, R., Naik, N., Clement, A., Gordon, N., & Miller, J.: Air–Sea  
647 Interaction and the Seasonal Cycle of the Subtropical Anticyclones. *J. Climate*, 16, 1948–  
648 1966, 2003.
- 649 Seinfeld, J.H. and Pandis, S.N.: Atmospheric Chemistry and Physics: From Air Pollution to  
650 Climate Change. 2nd Edition, John Wiley & Sons, New York, 2006.
- 651 Seinfeld, J. H., Bretherton, C., Carslaw, K. S., Coe, H., DeMott, P. J., Dunlea, E. J.,  
652 Feingold, G., Ghan, S., Guenther, A. B., Kahn, R., Kraucunas, I., Kreidenweis, S. M.,  
653 Molina, M. J., Nenes, A., Penner, J. E., Prather, K. A., Ramanathan, V., Ramaswamy, V.,  
654 Rasch, P. J., Ravishankara, A. R., Rosenfeld, D., Stephens, G., and Wood, R.: Improving



- 655 our fundamental understanding of the role of aerosol–cloud interactions in the climate  
656 system, *Proc.Nat.Acad.Sci.*, 113 (21) 5781-5790; doi:10.1073/pnas.1514043113, 2016.
- 657 Sinha, P., Hobbs, P. V., Yokelson, R. J., Bertschi, I. T., Blake, D. R., Simpson, I. J., and  
658 Gao, S.: Emissions of trace gases and particles from savanna fires in southern Africa, *J.*  
659 *Geophys. Res.*, 108, 8487, doi:10.1029/2002JD002325, D13, 2003.
- 660 Spracklen, D. V., Carslaw, K. S., Pöschl, U., Rap, A., and Forster, P. M.: Global cloud  
661 condensation nuclei influenced by carbonaceous combustion aerosol, *Atmos. Chem. Phys.*,  
662 11, 9067-9087, doi:10.5194/acp-11-9067-2011, 2011.
- 663 Thornhill, K. L., Anderson, B. E., Barrick, J. D. W., Bagwell, D. R., Friesen, R., and  
664 Lenschow, D.: Air motion intercomparison flights during Transport and Chemical  
665 Evolution in the Pacific (TRACE-P)/ACE-ASIA. *Journal of Geophysical Research*. 108.  
666 10.1029/2002JD003108, 2003.
- 667 Twomey, S.: Pollution and the Planetary Albedo, *Atmos. Env.*, 8, 1251-1256,  
668 doi:10.1016/0004-6981(74)90004-3, 1974.
- 669 Twomey, S.: The Influence of Pollution on the Shortwave Albedo of Clouds, *J. Atmos.*  
670 *Sci.*, 34, 1149–1152, doi:10.1175/1520-0469(1977)034<1149:TIOPOT>2.0.CO;2, 1977.
- 671 van der Werf, G. R., Randerson, J. T., Giglio, L., Collatz, G. J., Mu, M., Kasibhatla, P. S.,  
672 Morton, D. C., DeFries, R. S., Jin, Y., and van Leeuwen, T. T.: Global fire emissions and  
673 the contribution of deforestation, savanna, forest, agricultural, and peat fires (1997–2009),  
674 *Atmos. Chem. Phys.*, 10, 11707-11735, doi:10.5194/acp-10-11707-2010, 2010.
- 675 Yamaguchi, T., G. Feingold, J. Kazil, and A. McComiskey, A.: Stratocumulus to cumulus  
676 transition in the presence of elevated smoke layers, *Geoph. Res. Lett.*, 42, 10,478–  
677 10,485,doi:10.1002/2015GL066544, 2015.
- 678 Zhang, J. and Zuidema, P.: Low cloud reduction within the smoky marine boundary layer  
679 and the diurnal cycle, *Atmos. Chem. Phys. Discuss.*, <https://doi.org/10.5194/acp-2019-448>,  
680 in review, 2019.
- 681  
682 Zuidema, P., Sedlacek, A. J. III, Flynn, C., Springston, S., Delgadillo, R., Zhang, J., et al.:  
683 The Ascension Island boundary layer in the remote southeast Atlantic is often smoky.  
684 *Geoph. Res. Lett.*, 45, 4456–4465, doi:10.1002/2017GL076926, 2018.
- 685



686 **Tables**

687 **Table 1:** Average marine boundary layer (MBL) aerosol concentrations from the UHSAS,  
 688 CCN activity derived from in-situ CCN measurements ( $\kappa_{CCN}$ ) and bulk chemical  
 689 composition ( $\kappa_{AMS}$ ), and characteristic vertical updraft velocity ( $w^*$ ). Aerosol conditions are  
 690 classified for each flights as “polluted”, “intermediate”, or “clean” based on the MBL  
 691 aerosol concentration.

Flight Number	Date	Pollution Category	Aerosol Number (cm <sup>-3</sup> )	CFSTGC Operation Mode	$\kappa_{CCNc}$	$\kappa_{AMS}$	$w^*$ (ms <sup>-1</sup> )
RF01	12 Aug 17	Polluted	707 ± 104	Both <sup>§</sup>	0.4	-	0.45
RF02	13 Aug 17	Polluted	1012 ± 98	Both <sup>§</sup>	0.4	0.4	0.39
RF03	15 Aug 17	Intermediate	481 ± 109	SFCA <sup>^</sup>	0.4	0.4	0.44
RF08	24 Aug 17	Intermediate	493 ± 40	Both <sup>§</sup>	0.3	0.4	0.29
RF09	26 Aug 17	Intermediate	433 ± 34	CF <sup>*</sup>	0.4	0.4	0.45
RF10	28 Aug 17	Clean	205 ± 21	CF <sup>*</sup>	0.3	-	0.32
RF11	30 Aug 17	Clean	278 ± 24	Both <sup>§</sup>	0.2	0.4	0.26
RF12	31 Aug 17	Clean	195 ± 21	CF <sup>*</sup>	0.4	0.4	0.3 <sup>#</sup>

692 <sup>\*</sup> CF: Constant Flow operation of the CCN instrument.

693 <sup>^</sup> SFCA: Scanning Flow CCN Analysis operation of the CCN instrument.

694 <sup>§</sup> Both operation modes (CF, SFCA) of the CCN instrument were used.

695 <sup>#</sup>  $w^*=0.3$  ms<sup>-1</sup> assumed when calculating droplet number. This value was selected based  
 696 on the pollution category and date, and the average of corresponding  $w^*$  determined from  
 697 RF10, RF11.

698

699

700



701 **Figures Captions**

702

703 **Figure 1:** Map of ORACLES 2017 research flights used in this work, together with  
704 MODIS imagery of savannah fires throughout August 2017. Most flights are in close  
705 proximity to the “routine” flight path of due South along 5°E Longitude.

706

707 **Figure 2:** Vertical profiles (altitude in meters) of CCN concentration ( $\text{cm}^{-3}$ ) from 0.1% to  
708 0.4% supersaturation for all flights in this work.

709

710 **Figure 3:** Top panel: Predicted droplet number ( $N_d$ ;  $\text{cm}^{-3}$ ) and measured CCN ( $\text{cm}^{-3}$ ) at  
711 0.1% supersaturation as functions of marine boundary layer aerosol concentration ( $N_a$ ;  $\text{cm}^{-3}$ )  
712  $^3$ ) for all flights. Bottom panel:  $N_d$  against  $N_a$  in the MBL for all flights, colored by  
713 maximum in-cloud supersaturation ( $S_{max}$ ).

714

715 **Figure 4:** The sensitivity of droplet number to a) aerosol number ( $\partial N_d / \partial N_a$ ), b)  
716 characteristic velocity ( $\partial N_d / \partial w^*$ ), and, c) hygroscopicity parameter ( $\partial N_d / \partial \kappa$ ) as functions of  
717  $N_a$  ( $\text{cm}^{-3}$ ). The data is clustered using the “polluted”, “intermediate”, and “clean” groupings  
718 of Table 1.

719

720 **Figure 5:** Characteristic velocity,  $w^*$ , in the MBL as a function of  $N_a$  ( $\text{cm}^{-3}$ ) in the BBOA  
721 plume (blue) and in the MBL (red), for each flight.

722



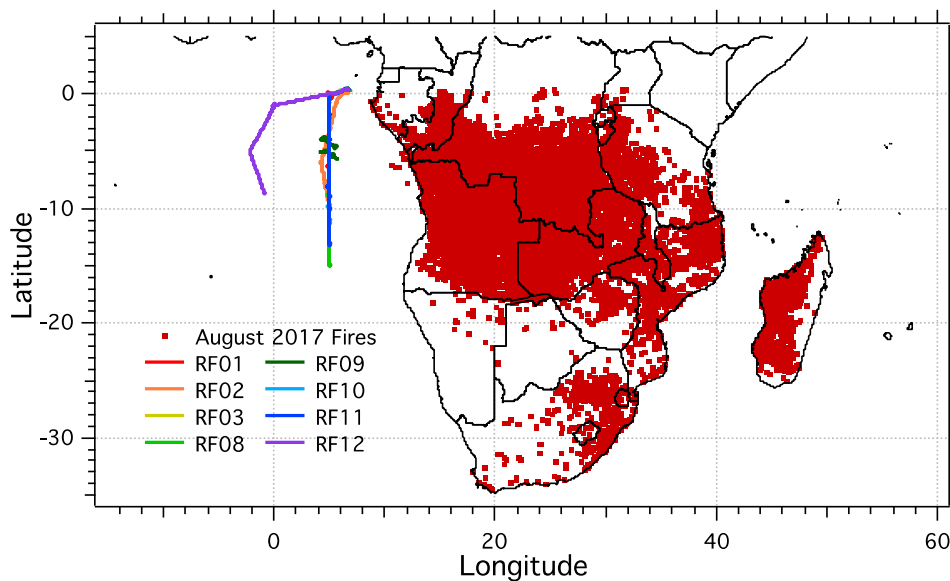
723 **Figure 6:**  $N_d^{lim}$  ( $\text{cm}^{-3}$ ) for each flight as a function of characteristic vertical updraft velocity,  
724  $w^*$  ( $\text{ms}^{-1}$ ). Flights are colored by “polluted”, “intermediate”, and “clean” categories, as  
725 defined by MBL concentration. The inset also presents the “asymptotic” activated droplet  
726 number ( $N_d^{lim}$ ;  $\text{cm}^{-3}$ ) for  $w^*$  ranging from 0.1 to 0.6  $\text{ms}^{-1}$ .

727

728 **Figure 7:** Spatial context of MBL aerosol for August 2017. Marker size as a function of  
729  $N_a$  ( $\text{cm}^{-3}$ ) and color as a function of  $N_d$  ( $\text{cm}^{-3}$ ).

730

731

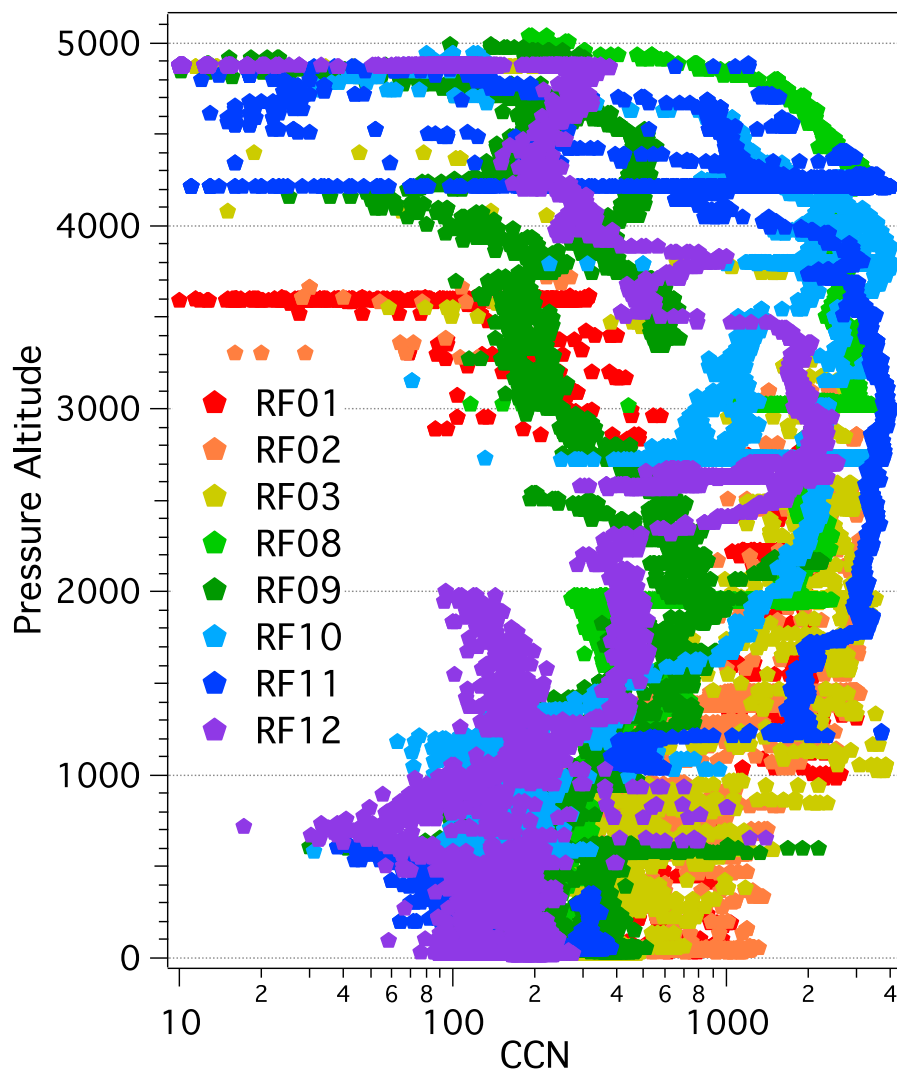


732

733 **Figure 1**

734

735



736

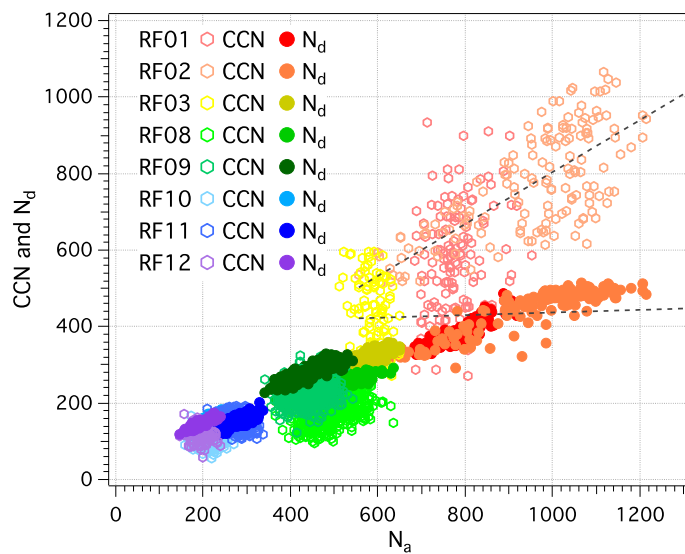
737

738 **Figure 2**

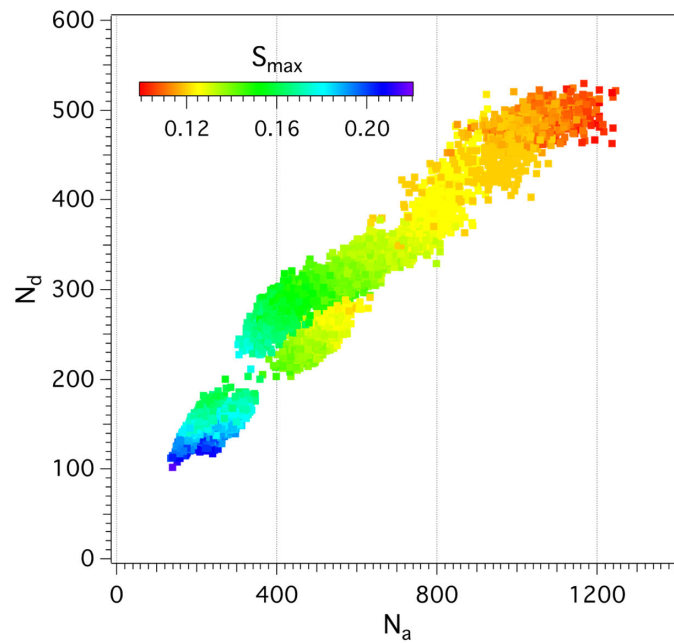
739

740





741



742

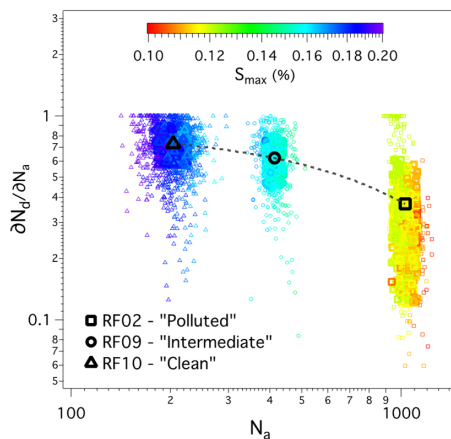
743

744 **Figure 3**

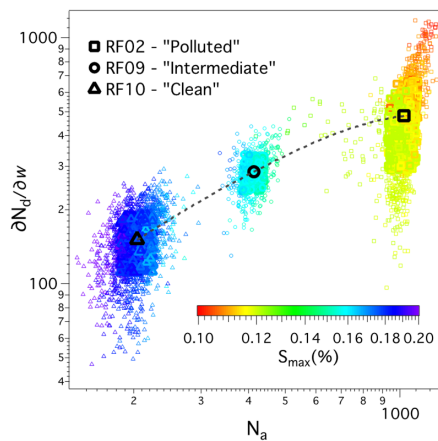
745



746



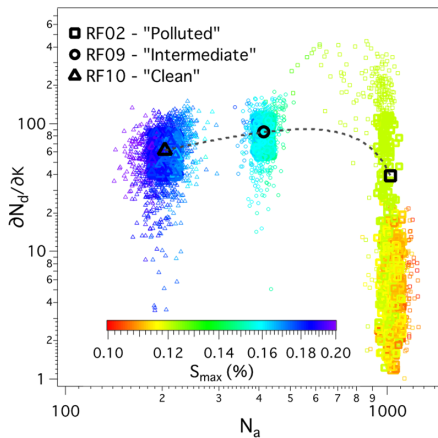
747

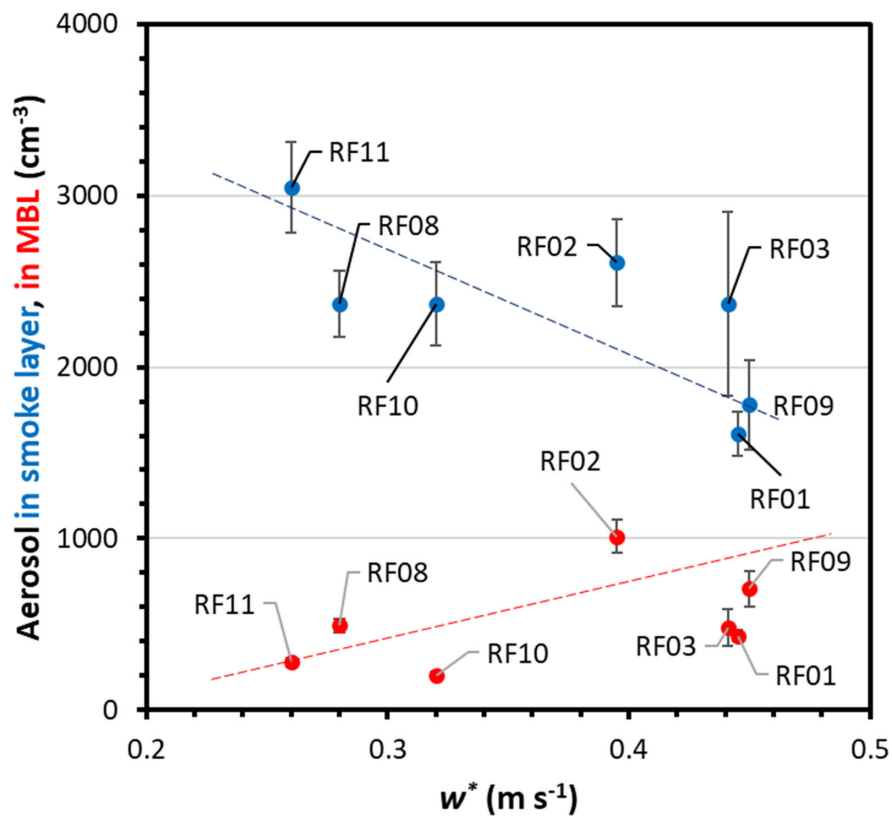


748

749 **Figure 4**

750



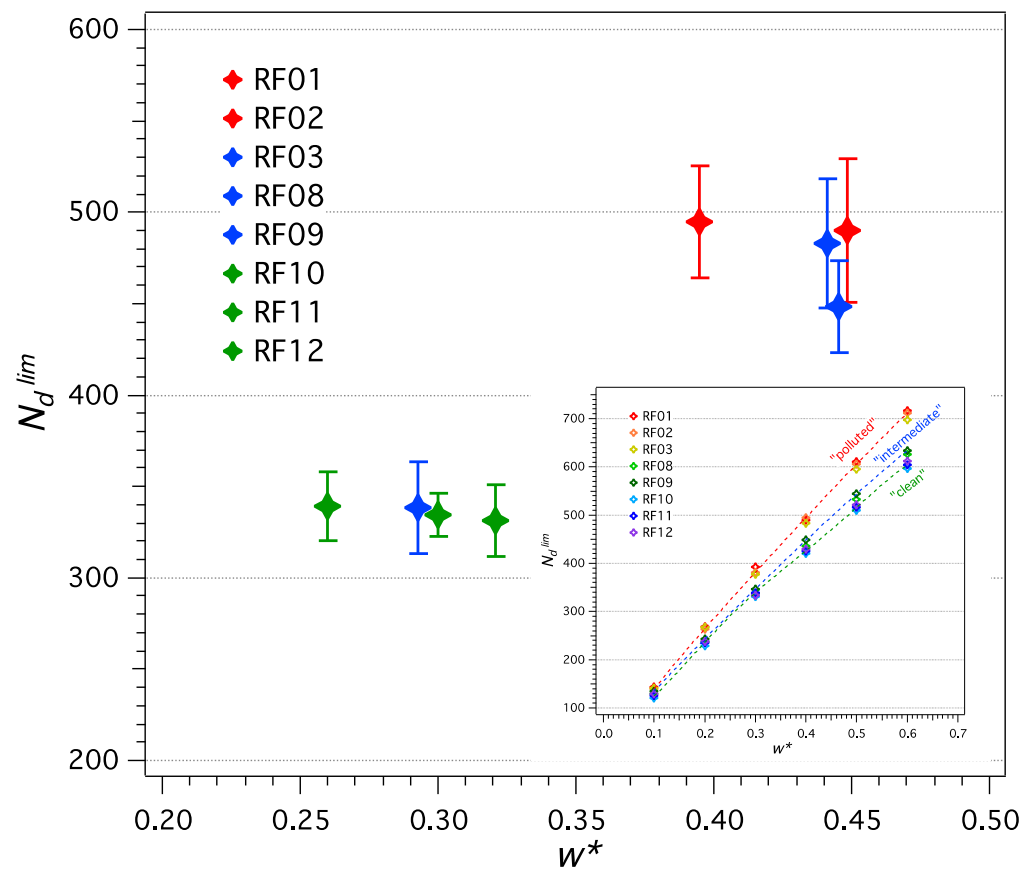


751

752 **Figure 5**

753

754



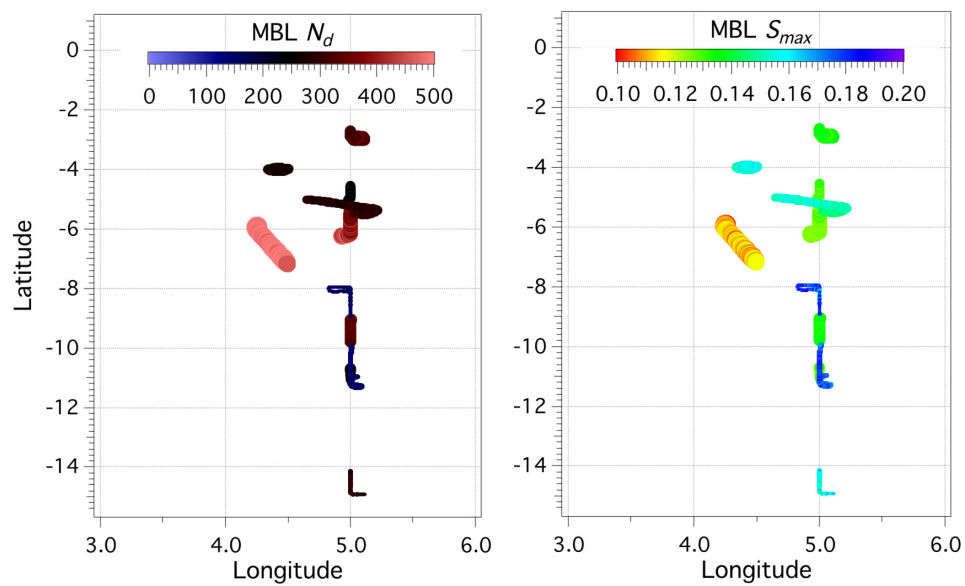
755

756

757 **Figure 6**

758

759



760

761 **Figure 7**

762

763

764